ACS APPLIED MATERIALS & INTERFACES

Research Article

www.acsami.org

Versatile Matrix for Constructing Enzyme-Based Biosensors

Zhaohao Wang,[†,§] Xi Luo,[†] Qijin Wan,*[,†] Kangbing Wu,[∥] and Nianjun Yang*[,†,‡]

[†]School of Chemistry and Environmental Engineering, Wuhan Institute of Technology, Wuhan 430073, China

[∥]School of Chemistry and Chemical Engineering, Huazhong University of Science and Technology, Wuhan 430074, China

[‡]Institute of Materials Engineering, University of Siegen, Siegen 57076, Germany

ABSTRACT: A versatile matrix was fabricated and utilized as a universal interface for the construction of enzyme-based biosensors. This matrix was formed on the gold electrode via combining self-assembled monolayer of 2,3-dimercaptosuccinic acid with gold nanoparticles. Gold nanoparticles were electrochemically deposited. Electrochemistry of three redox enzymes (catalase, glucose oxidase, and horseradish peroxidase) was investigated on such a matrix. The electrocatalytic monitoring of hydrogen peroxide and glucose was conducted on this matrix after being coated with those enzymes. On them the monitoring of hydrogen peroxide and glucose shows rapid response times, wide linear working ranges, low detection limits, and high enzymatic affinities. This matrix is thus a versatile and suitable platform to develop highly sensitive enzyme-based biosensors.

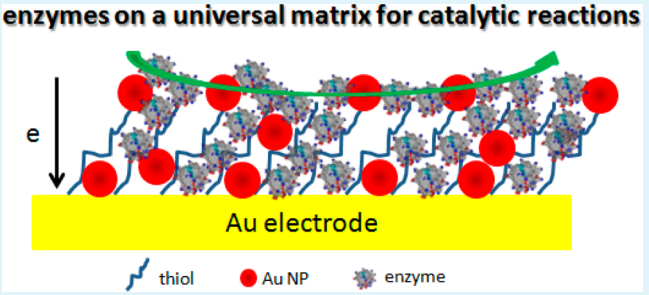

KEYWORDS: *versatile matrix, redox enzyme, gold nanoparticles, hydrogen peroxide biosensors, self-assembled monolayers*

INTRODUCTION

Developing versatile and simple matrixes have been paid extensive attention in past decades in that these matrixes are perfect interfaces to immobilize biomolecules (e.g., DNA, enzymes, proteins) and eventually to construct highly sensitive biosensors.[1−11] Self-assembled monolayer-based interfaces have been widely utilized as they provide highly ordered molecular assemblies and they are convenient, flexible, and simple systems.[4−17] Moreover, the formation of these monolayers is highly reproducible and reliable. In this way interfacial properties will be altered, resulting in artificially built environments at micrometer to nanometer scales. In these environments, biological activities of biomolecules (e.g., direct electron-transfer process and electrocatalytic ability) can be achieved.[4−11] In most cases, these layers act as binders to connect substrate electrodes with biomolecules. Furthermore, the biological activity (e.g., the electron-transfer rate) of biomolecules is designable as required by controlling the orientation and density of biomolecules via altering the types and the number of self-assembled monolayers.[4−17]

Combination of self-assembled monolayers of thiols with nanomaterials has been widely accepted as a standard method to build matrixes for the immobilization of biomolecules. Various nanomaterials such as metal nanoparticles, carbon nanotubes, graphene, silica nanoparticles, and other semiconductor nanoparticles (NPs) have been extensively used.[18−30] Among them, gold nanoparticles have been paid intensive attention[23−26] because of the advantages of facile control of their sizes and surfaces, easy synthesis protocols, excellent catalytic ability, and their high biocompatibility.[27−30] Different from flat planar electrodes, those matrixes constructed with self-assembled monolayers and nanomaterials always show three-dimensional structures. On them direct electron-transfer processes of redox enzymes as well as highly efficient catalytic abilities of enzymes (e.g., for electrocatalytic monitoring of small-sized biomolecules like hydrogen peroxide, and glucose) have been achieved.[30−40] Because of deeply buried redox centers inside enzymes, those activities are difficult to be achieved on flat planar electrodes. However, those three-dimensional matrixes make the orientation of enzymes possible and the denaturation of enzymes difficult, resulting in the realization of fast electron transfer of enzymes and their high electrocatalytic activities. Therefore, they possess more features than individual self-assembled monolayers of thiols as well as nanoparticles-based interfaces/matrixes for the immobilization of enzymes and other biomolecules. The disadvantage of those matrixes is that sometimes the matrixes might introduce interferences during the monitoring. In most cases, the matrixes are applied only for the realization of a direct electron-transfer process of one enzyme and its electrocatalytic activity.

Instead of the realization of direct electrochemistry of one enzyme on one matrix, we concentrate on designing one universal matrix for the achievement of direct electrochemistry of different enzymes. In this paper, we pay special attention to investigating the reduction behavior of different enzymes on one matrix. Herein, we report a technology to fabricate a versatile matrix that allows for the favorable immobilization of enzymes and eventually provides a suitable platform for sensing

Received: August 14, 2014
Accepted: September 10, 2014
Published: September 10, 2014

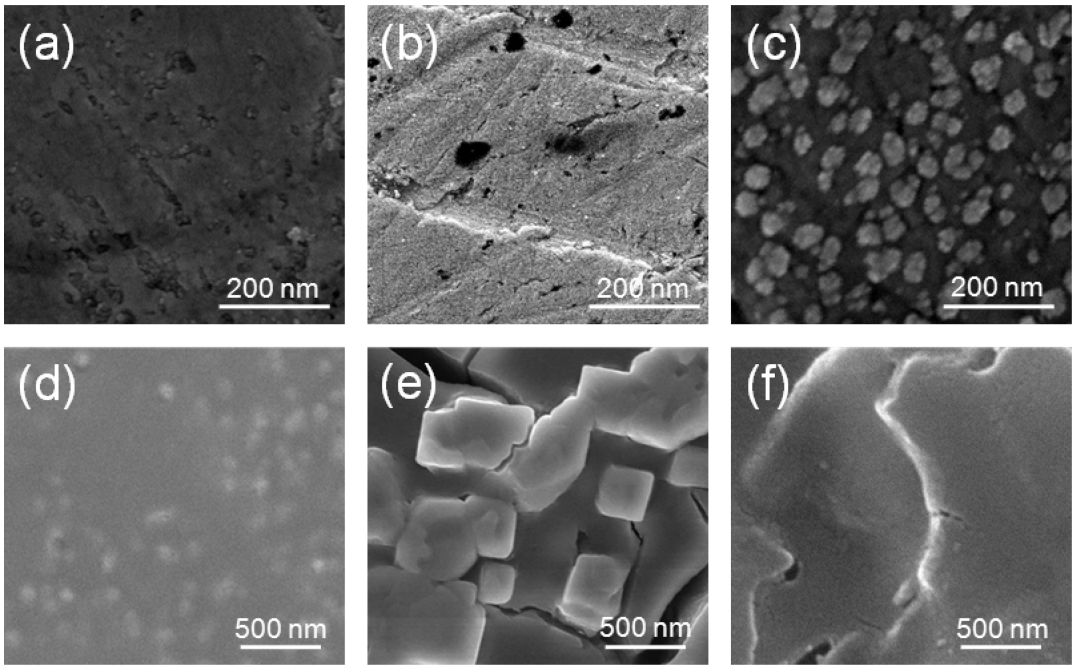

Figure 1. SEM images of a bare gold electrode before (a) and after being coated with a self-assembled monolayer of DMSA (b) and after being coated with gold nanoparticles and self-assembled monolayer of DMSA (c). Images (d), (e), and (f) are the matrix shown in (c) after being coated with CAT, GOD, and HRP, respectively.

small-sized biomolecules, hydrogen peroxide, and glucose. The matrix was constructed by marrying self-assembly monolayers with gold nanoparticles. Self-assembled monolayer was formed on the gold electrode using 2,3-dimercaptosuccinic acid (DMSA). Gold nanoparticles were in situ electrochemically deposited. On such a matrix, electrochemistry of three enzymes, catalase (CAT), glucose oxidase (GOD) and horseradish peroxidase (HRP), was investigated. After immobilization of those enzymes on the matrix, their electrocatalytic activities toward the reduction/oxidation of hydrogen peroxide and glucose were tested and compared.

EXPERIMENTAL SECTION

Chemical and Solutions. CAT (>100 units mg^{-1}), HRP (RZ-3, 250 units mg^{-1}), GOD (>100 units mg^{-1}), 3-mercapto-propionic acid (MPA), 2-mercaptosuccinic acid (MSA), and DMSA were obtained from Aladdin Regents Co. Ltd. (Shanghai, China) and used as-received. Other chemicals were purchased from Sinopherm Chemical Reagent Co. Ltd. (Shanghai, China). Hydrogen peroxide (H_2O_2) solutions were prepared freshly prior to experiments.

Instruments. Scanning electron microscopy (SEM) was performed with a Quanta 200 microscope (FEI Company, Eindhoven, The Netherlands). Atomic force microscopic (AFM) images were recorded on a Veeco Multimode Nanoscope V microscope (Veeco, Plainview, NY, USA). Electrochemical experiments were conducted on a CHI 660C electrochemical workstation (Shanghai Chenhua Apparatus Corporation, Shanghai, China) with a conventional three-electrode system at room temperature. A platinum foil was used as the auxiliary electrode and a saturated calomel electrode acted as the reference electrode. The working electrode was either a bare gold disk electrode (2.0 mm diameter) or a modified gold electrode.

Electrode Fabrication. The matrix (Au NPs/DMSA/Au) was fabricated in the following way: (i) Cleaning the gold electrode in a Piranha solution (concentrated H_2SO_4 and H_2O_2 with a volume ratio of 3:1) (*CAUTION: Piranha solution is quite corrosive, so please handle this solution with extreme care*); (ii) activating the electrode via cycling in the potential range of 0−1.0 V at a scan rate of 0.1 V s^{-1} in 0.5 M H_2SO_4 for more than 10 cycles (until a reproducible cyclic voltammogram is recorded); (iii) self-assembling of DMSA by immersing the electrode in a freshly prepared 20 mM DMSA solution for 12 h (to optimize the formation of the self-assembled monolayers on the gold electrode, 20 mM MSA and MPA were applied as well); (iv) depositing gold nanoparticles by applying −0.15 V on the electrode for 90 s in 4 mg mL^{-1} $HAuCl_4$ solution. For each step, the electrode was washed carefully and copiously with water. The immobilization of enzyme was done by drop-casting 4−10 μL of 5 mg mL^{-1} enzyme solutions on the surface of an Au NPs/DMSA/Au electrode. These enzyme electrodes were stored in 0.1 M pH 7.4 phosphate buffer at 4 °C when they were not in use.

RESULTS AND DISCUSSION

Figure 1a shows a SEM image of a clean gold electrode with a view of the uneven surface. This is a typical SEM image of a gold electrode after polishing and electrochemical treatments. The surface (Figure 1b) becomes glossy after its coating with DMSA. The cluster on the surface is due to the isolative DMSA organic molecule layers. Figure 1c shows the SEM image of the surface in Figure 1b but after electrochemical deposition of gold nanoparticles. A deposition potential of −0.15 V and a deposition time of 90 s were used. The gold nanoparticles are round-shaped and well-separated with an average diameter of about 40−80 nm. The surface is not fully covered by gold nanoparticles and a three-dimensional structure is achieved. This is due to favorable and continuous growth of gold nanoparticles on the surface. This is actually a proof of efficient/short conduction pathways for electron transfer during deposition. On the other side, it is known that the surface terminal groups (e.g., carboxyl, carbonyl, and hydroxyl groups) of a self-assembled monolayer act as anchoring sites for growing/depositing metal nanoparticles. Therefore, in our case, the carboxyl terminal functional group in the DMSA is an anchoring site for the growth of gold nanoparticles, providing the pathway of electron transfer. Please note here that the size of DMSA is much smaller than gold nanoparticles grew; more works are definitely required by AFM or scanning tunneling

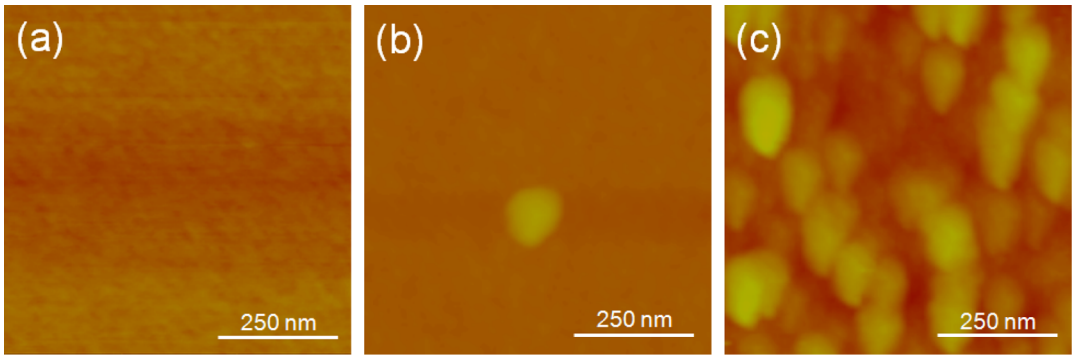

Figure 2. Tapping mode AFM images of a bare gold electrode (a) before and after being coated with a self-assembled monolayer of DMSA (b) and after being coated with gold nanoparticles and self-assembled monolayer of DMSA (c).

microscope (STM) in liquid at early stages of the growth of gold nanoparticles. The selection of thiol is discussed in a later session. The surface in Figure 1c is rougher than those in Figure 1a,b. For trapping enzymes such as CAT, GOD, and HRP, such a rough surface, a so-called matrix shown in Figure 1c, brings a more active area to touch with enzymes, leading to their facile and efficient electron-transfer processes.[31−35] Parts (d)−(f) of Figure 1 show three example SEM images of such a matrix after being coated with CAT (d), GOD (e), and HRP (f), respectively. The SEM image of the matrix coated with CAT (Figure 1d) shows that a smooth and close but transparent membrane forms on the surface. Gold nanoparticles are vaguely seen under the film in this case. When the electrode is coated with GOD, scattered crystalline particles are clearly seen (Figure 1e), instead of a thin and transparent membrane as shown in Figure 1d. HRP layer coated on such an electrode (Figure 1f) appears with some cracks. It is however much smoother and thicker than that in Figure 1d. Thus, gold nanoparticles underneath cannot be seen anymore. Although these images (Figure 1d−f) in dry states do not give us any information about the activities and conformation states of these enzymes, they confirm their successful coating on such a matrix.

Coating the gold electrode with self-assembled monolayer of DMSA and gold nanoparticles was checked further with a tapping mode atomic force microscope (AFM). For these experiments, a 200 nm gold film was sputtered on a silicon substrate and used as the electrode. As clearly seen from AFM images in Figure 2a,b, the gold electrode surface (Figure 2a) is pretty smooth, even after being coated with DMSA (Figure 2b). The big particle in Figure 2b is probably the cluster of isolative DMSA organic molecules, the same as that observed in the SEM image (Figure 1b). After electrochemical under-potential deposition of gold nanoparticles, the surface becomes rough and many round particles are seen (Figure 2c). These nanoparticles are well-distributed over the surface, presenting a three-dimensional structure. Their mean diameter is approximately 60−80 nm, which is in good agreement with the SEM results. Such a three-dimensional structure, so-named a matrix, is promising to retain enzymes for a long period of time and to improve their electrochemical activity.

The interface properties of such a matrix were investigated using cyclic voltammetry. Redox couple of $[Fe(CN)_6]^{3-/4-}$ were applied as the probes. Figure 3A shows representative voltammograms on different electrodes, including a bare gold electrode (Figure 3A-a), a DMSA-layer-coated gold electrode (DMSA/Au, Figure 3A-b), and a DMSA/Au electrode coated

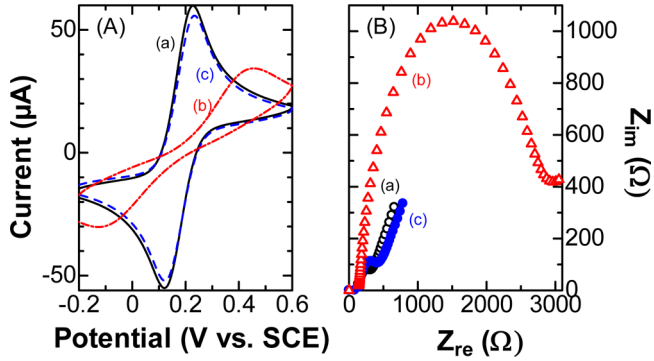

Figure 3. Cyclic voltammograms (A) and Nyquist plots (B) of 1.0 mM $Fe(CN)_6^{3-/4-}$ on a bare gold electrode (a), a DMSA/Au electrode (b), and an Au NPs/DMSA/Au electrode (c) in 0.1 M KCl solution. The scan rate is 0.1 V s^{-1}. The Nyquist plots were recorded at open circuit potentials.

with gold nanoparticles (Au NPs/DMSA/Au, Figure 3A-c). On a bare electrode, a pair of symmetric redox peaks with a peak separation of 95 mV is seen. After the introduction of DMSA, the peak separation enlarges to 390 mV. The peak currents of both anodic and cathodic waves decrease remarkably, indicating reduced electron-transfer rate of the redox reaction of $[Fe(CN)_6]^{3-/4-}$. This indicates the formation of a self-assembled monolayer of DMSA on the surface of the gold electrode. Further deposition of gold nanoparticles on the DMSA/Au electrode on the contrary leads to the values of peak separation and peak currents back to those obtained on a bare gold electrode. An Au NPs/DMSA/Au electrode thus provides fast and facile electron-transfer paths for the redox reaction of $[Fe(CN)_6]^{3-/4-}$.

The properties of such a matrix were then examined with electrochemical impedance spectroscopy in 1.0 mM $[Fe(CN)_6]^{3-/4-}$ at open circuit potentials. Figure 3B shows the Nyquist plots on these electrodes. Semicircles at higher frequencies and linear portions at low frequencies are noticed, suggesting electron-transfer limited diffusion processes. The electron-transfer resistance (R_{CT}) was evaluated from the diameter of the semicircle. R_{CT} value for a bare gold electrode is about 125 Ω (Figure 3B-a). For a DMSA/Au electrode, R_{CT} increases to 1000 Ω (Figure 3B-b). This is due to the well-known block effect of thiol monolayer on the electrode. R_{CT} of an Au NPs/DMSA/Au electrode reduces from 1000 to 190 Ω (Figure 3B-c), indicating that gold nanoparticles behave as new reactive sites and accelerate the electron-transfer rate of the redox reaction of $[Fe(CN)_6]^{3-/4-}$.[34−36] An Au NPs/DMSA/Au

electrode is thus a promising matrix for the electrochemistry of enzymes because it has not only a three-dimensional structure (from SEM and AFM results), but also provides the smallest electron-transfer resistance.

Electrochemistry of CAT was tested on such a matrix (an Au NPs/DMSA/Au electrode). The voltammogram of CAT in 0.1 M pH 7.4 phosphate buffer is shown in Figure 4A-a. A good-

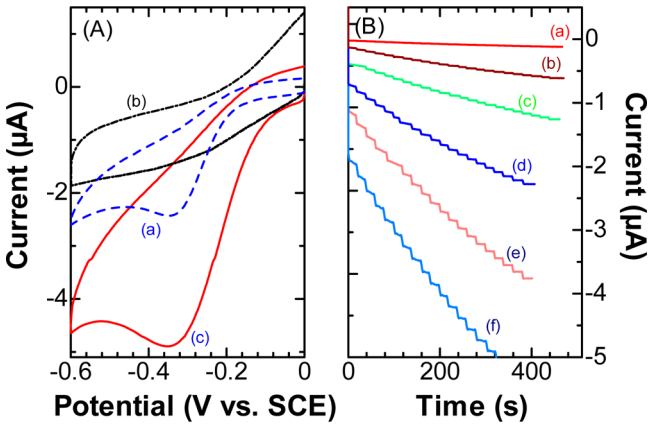

Figure 4. (A) Cyclic voltammograms in 0.1 M pH 7.4 phosphate buffer on an Au NPs/DMSA/Au electrode (a) and a CAT/Au NPs/DMSA/Au electrode before (b) and after adding 0.8 mM hydrogen peroxide (c). The scan rate was 0.1 V s^{-1}. (B) Amperometric curves of a CAT/Au NPs/DMSA/Au electrode in 0.1 M pH 7.4 phosphate buffer after the successive addition of 40 μM hydrogen peroxide at an operation potential of −0.2 (a), −0.3 (b), −0.35 (c), −0.4 (d), −0.45 (e), and −0.5 (f) V.

shaped reduction peak is observed at −0.35 V. As a control experiment, the voltammogram of this matrix in the buffer was recorded. As shown in Figure 4A-b, no redox peaks are seen in the scanned potential range. The electrode reaction of CAT on such a matrix was investigated by recording cyclic voltammograms at different scan rates. The peak current increases proportionally with an increase of scan rates in the range of 0.02−0.25 V s^{-1}. The peak potential shifts negatively as well. The redox reaction of CAT on such a matrix is thus an adsorption-controlled process. The surface coverage of CAT on such a matrix was calculated to be 2.7×10^{-11} mol cm^{-2} and the apparent heterogeneous electron-transfer rate constant (k_s) was calculated to be 2.96 s^{-1} when a charge-transfer coefficient of 0.5 was used. Electrocatalytic reduction of hydrogen peroxide was also tested using immobilized CAT on such a matrix. The resulted voltammogram is shown in Figure 4A-c. After the addition of 0.8 mM hydrogen peroxide, the reduction current increased significantly, indicating high catalytic activity toward the reduction of hydrogen peroxide. Therefore, the peak at −0.35 V shown in Figure 4A-a is due to the redox reaction of CAT.

It is well-known that hydrogen peroxide and glucose biosensors are important for pharmaceutical, clinical, and environmental, and related applications.[42−51] The performance of those biosensors however strongly relied on the electrode materials/structures (e.g., glassy carbon electrode, graphene, carbon nanotubes, and TiO_2) and/or the selected catalysts (e.g., enzymes and metal nanoparticles). It is thus highly desirable to develop a reliable and universal matrix to construct hydrogen peroxide and glucose biosensors. In addition to providing a good environment for efficient enzyme loading and maintenance of enzyme bioactivity, this matrix, namely, an Au NPs/DMSA/Au electrode shown above, seems to be promising for the sensitive detection of hydrogen peroxide. Amperometry was then applied for the detection of hydrogen peroxide on the CAT-coated matrix (CAT/Au NPs/DMSA/Au). Figure 4B shows amperometric curves on the CAT/Au NPs/DMSA/Au matrix after adding continuously 40 μM hydrogen peroxide. The working/operation potential was varied from −0.2 V (Figure 4B-a), −0.3 V (Figure 4B-b), −0.35 V (Figure 4B-c), −0.4 V (Figure 4B-d), −0.45 V (Figure 4B-e), to −0.5 V (Figure 4B-f). More negative working potentials lead to higher reduction currents. Considering the effect of oxygen and other species (e.g., desorbed thiols at negative potentials) in solutions, we chose −0.35 V for the detection of hydrogen peroxide. The pH value of the phosphate buffer affects the amperometric response as well. Too low or too high pH values are not so perfect for the detection of hydrogen peroxide. When the pH value is higher than 7.4, the response slows

Table 1. Analytical Characteristics of Different Matrixes toward the Detection of Hydrogen Peroxide

electrode	linearity (μM)	LOD (μM)	sensivity (μA mM^{-1} cm^{-2})	K_M^{app} (mM)	reference
CAT/Au NPs/DMSA	3−5860		16.4	0.57	this work
CAT/nanoNiO/MWCNTs	200−2530		337.58	1.68	42
CAT/nanoFe_3O_4/Au	1.5−13.5				43
CAT/Pt	1−90		32.5		44
CAT/Au NPs/GR−NH_2	0.3−600	0.05	13.4	2.81	39
CAT/SWNT−CHI	5−50	2.5	6.32		45
CAT/cysteine/Si sol−gel	1−30	0.4			46
GOD/Au NPs/DMSA	2−3500	0.65	12.4	1.0	this work
HRP/Au NPs/DMSA	2−2860	0.7	7.2	0.59	this work
HRP/3-MPT	0.5−100	0.1			47
HRP/poly/Au NPs	5−1100	1.5	0.498	1.01	49
HRP/DNA−Ag NPs/Au NPs/DNA−Ag	7−7800			1.3	48
HRP/SiO_2/BSA/Au NPs	8−3720			2.3	40
HRP/$CaCO_3$−Au NPs	0.5−5200	0.1			10
HRP−Au NPs/ALG	20−13700		40.1	9.3	41

MWCNT, multiwalled carbon nanotubes; GR−NH_2, amine-functionalized graphene; SWNT, single-walled carbon nanotubes; CHI, chitosan; 3-MPT, (3-mercaptopropyl)trimethoxysilane; poly, polymer of aniline and boronic acid; Au NPs, gold nanoparticles; PDDA, poly(diallyldimethylammonium chloride); BSA, bovine serum albumin; Thio−Naf, thionine/nafion; ALG, sodium alginate.

down, although the current is still at a comparatively high level. The pH value lower than 6.0 results in smaller currents as well as longer response times. These results indicate that the activity of CAT on such a matrix is pH-dependent. We selected 0.1 M pH 7.4 phosphate buffer for the detection of hydrogen peroxide during subsequent experiments.

Amperometric curves were then recorded on the CAT/Au NPs/DMSA/Au electrode in 0.1 M pH 7.4 phosphate buffer when hydrogen peroxide at different concentrations was added. The working potential applied was −0.35 V. Typical steady-state amperometric curves were seen. The steady-state current in the amperometric curves is linear with the concentration of hydrogen peroxide in the range from 3.0 μM to 5.86 mM. The linear equation is I (μA) = $(3.9 \times 10^{-3})c$ (μM), where I is the absolute value of the steady-state current in μA and c is the concentration of hydrogen peroxide in μM. The correlation coefficient is 0.998 (n = 21) and the sensitivity is determined as 16.4 μA mM^{-1} cm^{-2}. A detection limit was calculated to be 2.0 μM (S/N = 3).

It is important to discuss the apparent Michaelis−Menten constant (K_M^{app}) because it reflects the enzymatic affinity and the ratio of microscopic kinetic constant. To obtain this value, we used the Lineweaver−Burk equation in the form[37,38]

$$\frac{1}{I_{ss}} = \frac{1}{I_{max}} + \frac{K_M^{app}}{I_{max}C} \quad (1)$$

where I_{ss} is the steady-state cathodic current after the addition of hydrogen peroxide, I_{max} is the maximum steady-state current measured under saturated hydrogen peroxide, and c is the concentration of hydrogen peroxide added into the buffer. By drawing a plot of $1/I_{ss}$ versus $1/c$, we found that the plot is much closer to a curve instead of a straight line. This fact indicates that the value of K_M^{app} is not constant but changes at different conditions. The variation of K_M^{app} as a function of the concentration of hydrogen peroxide might result from the loss and/or denaturation of CAT as well as from the interferences of thiols and gold nanoparticles. The best fitting line gives a slope of 0.0067, resulting in the value of K_M^{app} of 0.57 mM. This value is much lower than those reported,[39−42] indicating high catalytic activity of CAT on such a matrix toward the reduction of hydrogen peroxide.

Table 1 compares the achieved results on such a matrix with those published on other matrixes regarding the linearity, limit of detection (LOD), the sensitivity for the monitoring of hydrogen peroxide, and the value of K_M^{app}.[39−49] In the literature, various types of electrodes (e.g., gold electrode, glassy carbon electrode, and platinum electrode) have been used. To immobilize enzymes for the catalytic reduction of hydrogen peroxide, those electrodes were modified or functionalized with different nanomaterials (e.g., gold nanoparticles, nano NiO, carbon nanotubes, nano Fe_3O_4 particle, graphene, and DNA) through numerous approaches (e.g., direct coating/casting, self-assembling, and sol−gel methods). Depending on the used electrode, nanomaterials, enzymes, and the constructed electrode structure, the sensing performances (linearity, LOD, sensitivity, etc.) of hydrogen peroxide on those electrodes/matrixes vary greatly. For example, a pretty wide linear working range (from 20 μM to 13.7 mM) was reported with a detection limit of 3 μM on a HRP-Au NPs/ALG/Au electrode,[41] although the sensitivity (40.1 μA mM^{-1} cm^{-2}) is lower than those on the CAT/nanoNiO/MWCNTs/GCE matrix[42] and the HRP/DANN-Ag NPs/PDDA-Au NP matrix.[48] On our matrix, the K_M^{app} value is much smaller than those reported;[39,40,45−49] the linearity obtained is relatively wide (3 μM to 5.86 mM); the detection limit (LOD) is as low as 2 μM, which is lower than most of the reported results.[41,42,45] Although smaller K_M^{app} value (in other words high enzymatic affinities) was obtained, the sensitivity of our CAT/Au NPs/DMSA/Au matrix is required to be improved. In conclusion, the hydrogen peroxide sensor using the CAT/Au NPs/DMSA/Au matrix shows relatively better sensing performance than most developed sensors.

We further tested the electrochemistry of GOD on this matrix. Figure 5A shows the voltammetric responses of an Au

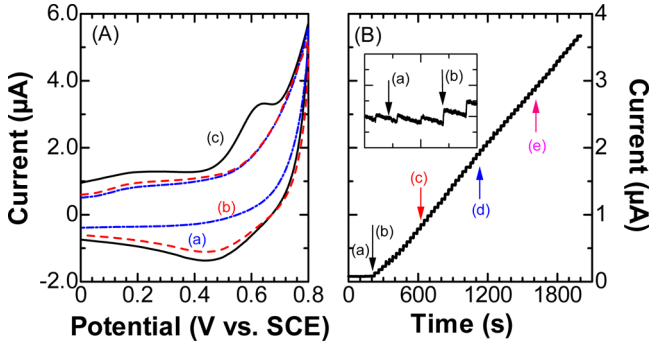

Figure 5. (A) Cyclic voltammograms in 0.1 M pH 7.4 phosphate buffer on the Au NPs/DMSA/Au electrode (a) and the GOD/Au NPs/DMSA/Au electrode before (b) and after adding 2.0 mM glucose (c). The scan rate was 0.1 V s^{-1}. (B) Amperometric responses of glucose on the GOD/Au NPs/DMSA/Au electrode in 0.1 M pH 7.4 phosphate buffer. The concentration of added glucose was 0.8 μM (a), 4.0 μM (b), 0.1 mM (c), 0.5 mM (d), and 1.0 mM (e). The operation potential was 0.6 V. The inset shows the amperometric response of the GOD/Au NPs/DMSA/Au electrode when 0.8 μM (a) and 4.0 μM (b) glucose were added.

NPs/DMSA/Au electrode before and after being coated with GOD (GOD/Au NPs/DMSA/Au) in 0.1 M pH 7.4 phosphate buffer. The voltammogram for an Au NPs/DMSA/Au electrode is featureless in the scanned potential range (Figure 5A-a). While a broad cathodic wave is seen at about 0.46 V on the GOD/Au NPs/DMSA/Au electrode (Figure 5A-b). Adding glucose into the buffer solution leads to the slight enhancement of cathodic current (Figure 5A-c). A pronounced anodic wave appears as well at about 0.64 V (Figure 5A-c), which is characteristic of electrochemical catalytic oxidization of glucose. The peak potential of the oxidation of glucose is more positive than those reported.[50,51] This is probably due to different properties of the electrode matrix.

It has been proven that GOD-based interfaces are ideal models for glucose sensing.[50,51] The electrocatalytic oxidation of glucose on the GOD/Au NPs/DMSA/Au matrix was conducted. Figure 5B shows one amperometric curve of the GOD/Au NPs/DMSA/Au matrix in 0.1 M pH 7.4 phosphate buffer after adding glucose with different concentrations. In the blank buffer a steady baseline is obtained during the first 100 s. The addition of 0.8 μM glucose (Figure 5B-a) into the blank buffer causes an obvious increase of the current. Within 5 s the current reaches 95% of the maximum value, indicating rapid oxidation of glucose on the GOD/Au NPs/DMSA/Au electrode. The steady-state current increases when the concentration of glucose enhances to 4.0 μM (Figure 5B-b), 0.1 mM (Figure 5B-c), 0.5 mM (Figure 5B-d), and 1.0 mM

Table 2. Analytical Characteristics of Different Matrixes toward the Detection of Glucose

electrode	linearity (μM)	LOD (μM)	selectivity (μA cm^{-2} mM^{-1})	K_M (mM)	reference
GOD/AuNPs/DMSA	0.8−4000	0.3	9.8	5.2	this work
GOD/Ch−AuNPs−Fe_3O_4	3.0−570	1.2			52
GOD/Pt/MWNT−PANI	3.0−8200	1.0	16.1	0.64	53
GOD/Nafion/ZnO−HNSPs	5.0−13150	1.0	65.82		54
GOD/AuNPs/MWCNT	20−10000	2.3	19.27	6.7	55
GOD/PdNPs/Ch−GR	1.0−1000	0.2	31.2		56
GOD/Ch/TiO_2/nanofiber		10	9.25		57
GOD/MWNT/Nafion	20−1020	10	13	2.2	58
GOD/MWNT−Ch/PB	25−1300	7.5	15.2	3.67	59
GOD/NiO	30−5000	24	0.446	2.7	60
GOD/nanoPANi	10−5500	0.3	97.18	2.37	61
GOD/silicaKIT-6	0−2830		7.29		62
GOD/BGMC	10−7490	10			63
GOD/PB/Bi_2Se_3	10−11000	3.8	24.55		64
GOD/GRNS−CNS	400−20000	100			65
GOD/PtNPs−CNT−Ch	1.2−2000	0.4	41.9	0.64	66
GOD/BC/Ni	25−1190	8.3		0.32	67
GOD/ZnO	100−9000	1.9		3.12	68
GOD/AuPdNPs	6.9−3500	6.9	2666.6	10.5	69
GOD/thiourea	up to 5500	6.0	5.73	3.42	70

Au NPs, gold nanoparticles; Ch, chitosan; MWCNT, multiwalled carbon nanotube; PANI, polyaniline; HNSPs, hollow nanospheres; Pd NPs, palladium nanoparticles; GR, graphene; PB, prussian blue; BGMC, bicontinuous gyroidal mesoporous carbon; GRNS, graphene nanosheet; CNS, carbon nanosheet; Pt NPs, platium nanoparticle; CNT, carbon nanotube; BC, boron-doped carbon; AuPdNPs, gold and palladium alloy nanoparticles.

(Figure 5B-e). A response plateau is noticed when the glucose concentration is higher than 4.0 mM, indicating a Michaelis−Menten kinetic mechanism. K_M^{app} was then estimated to be 5.2 mM. Under these conditions, the oxidation current is linear within the concentration of glucose in the range from 0.8 μM to 4.0 mM with a correlation coefficient of 0.9994 (n = 64). The sensitivity is 9.8 μA cm^{-2} mM^{-1} and the detection limit was calculated to be 0.3 μM (S/N = 3). As compared partially in Table 2, the sensing performance for the monitoring of glucose on the GOD/Au NPs/DMSA/Au matrix is relatively better than most of those reported[52−78] with respect to the linearity and LOD. For example, on a nanocomposite film prepared with iron oxide, gold nanoparticles, and chitosan, the linearity was 3.0 μM to 0.57 mM and LOD was 1.2 μM;[52] on a polymer/CNT nanocomposite the linearity and LOD was 3.2 μM to 8.2 mM and was 1.0 μM.[53] Layer-by-layer assembled GOD and thiourea on a glassy carbon electrode can detect glucose up to 5.5 mM.[70] Subsequently, with a GOD-coated matrix, the GOD/Au NPs/DMSA/Au electrode can be applied for sensitive detection of glucose.

Meanwhile, a clear cathodic peak appears at around −0.35 V on the GOD/Au NPs/DMSA/Au electrode (Figure 6A-a), which does not show up before coating the electrode with GOD (Figure 6A-b) in the buffer. Furthermore, the capacitive current increases dramatically. This demonstrates that the deeply buried redox center inside GOD has been partially contacted with the electrode due to the special three-dimensional structure of such a matrix.[25] The electrode reaction of GOD on such a matrix was investigated. The peak current proportionally increases with an increase of scan rates in the range of 0.02 to 0.2 V s^{-1}. The peak potential shifts negatively as well. The redox reaction of GOD on such a matrix is thus an adsorption-controlled process. The surface coverage of GOD on such a matrix was calculated to be 8.3 × 10^{-11} mol cm^{-2} and k_s was calculated to be 4.92 s^{-1} when a charge-transfer coefficient of 0.5 was used. Therefore, the redox reaction of GOD is realized on such a matrix.

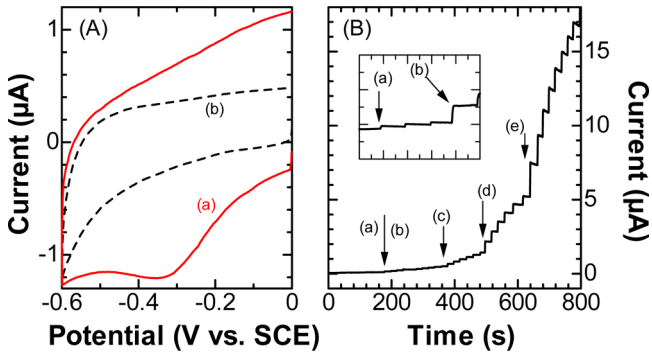

Figure 6. (A) Cyclic voltammograms of an Au NPs/DMSA/Au electrode (a) and a GOD/Au NPs/DMSA/Au electrode (b) in 0.1 M pH 7.4 phosphate buffer. The scan rate was 0.1 V s^{-1}. (B) Amperometric responses of the GOD/Au NPs/DMSA/Au electrode in 0.1 M pH 7.4 phosphate buffer after successive additions of hydrogen peroxide with concentrations of 2 (a), 10 (b), 40 (c), 200 (d), and 800 (e) μM. The operating potential was 0.3 V. The inset shows the amperometric response of the GOD/Au NPs/DMSA/Au electrode when 2 μM (a) and 10 μM (b) hydrogen peroxide was added.

We then further recorded the voltammograms on the GOD/Au NPs/DMSA/Au electrode after 1.5 mM hydrogen peroxide was added. Those tests had seldom been tried.[79] The oxidation current in the presence of hydrogen peroxide increases sharply when the scanning potential is above +0.2 V. Control experiments showed that none of the electrodes (e.g., an Au NPs/DMSA/Au electrode, a DMSA/electrode, and a bare gold electrode) made the oxidation current enhanced after adding hydrogen peroxide into the buffer. For the electrocatalytic determination of hydrogen peroxide at the GOD/Au NPs/DMSA/Au electrode, amperometry was then conducted. The

experimental conditions were optimized as follows: 0.1 M pH 7.4 phosphate buffer and a working potential of 0.3 V. Figure 6B shows one amperometric curve on the GOD/Au NPs/DMSA/Au matrix after successive addition of hydrogen peroxide with the concentration of 2 μM(Figure 6B-a), 10 μM (Figure 6B-b), 40 μM (Figure 6B-c), 200 μM (Figure 6B-d), and 800 μM (Figure 6B-e). The inset shows the enlargement of the amperometric curve of the GOD/Au NPs/DMSA/Au electrode when 2 μM (a) and 10 μM (b) hydrogen peroxide was added, manifesting high sensitivity of the electrocatalytic oxidation of hydrogen peroxide. Therefore, such an GOD/Au NPs/DMSA/Au matrix has excellent characteristics of the catalytic oxidation of hydrogen peroxide. Under these conditions, the steady-state current linearly increases with the concentration of hydrogen peroxide in the range of 2.0 μM to 3.5 mM. The linear equation is I (μA) = $(2.0 \times 10^{-4})c$ (μM), where I is the absolute value of the steady-state current in μA and c is the concentration of hydrogen peroxide in μM. The correlation coefficient is 0.996 (n = 32) and the sensitivity is determined as 12.4 μA mM^{-1} cm^{-2}. The detection limit was calculated to be 0.65 μM (S/N = 3). Furthermore, the value of K_M^{app} was calculated to be about 1.0 mM. These results confirm the suitability of such a matrix for enzyme immobilization and further for constructing enzyme-based hydrogen peroxide biosensors.

Electrochemistry of HRP was studied on an Au NPs/DMSA/Au electrode as well. On HRP-coated Au NPs/DMSA/Au electrode (HRP/Au NPs/DMSA/Au), a good-shaped reduction peak is observed at −0.45 V. Control experiment on an Au NPs/DMSA/Au electrode in the buffer is featureless. An increase of scan rates leads to linearly enhanced peak currents and negative shift of reduction potentials, indicating an adsorption-controlled electrode process. The surface coverage and k_s of HRP on Au NPs/DMSA/Au electrode was calculated to be 9.7×10^{-11} mol cm^{-2} and 5.96 s^{-1} (with a charge-transfer coefficient of 0.5), respectively. Adding hydrogen peroxide in the buffer results in a huge increase in the cathodic current of the HRP/Au NPs/DMSA/Au matrix. Figure 7A shows an amperometric curve on the HRP/Au NPs/DMSA/Au matrix when 2 μM (Figure 7A-a), 10 μM (Figure 7A-b), 40 μM (Figure 7A-c), 200 μM (Figure 7A-d), and 800 μM (Figure 7A-e) μM hydrogen peroxide is added. The steady-state current, obtained with an optimized working potential of −0.45 V in 0.1 M pH 7.4 phosphate buffer, increases when hydrogen peroxide with higher concentrations is added. Figure 7B shows the dependence of the steady-state current as a function of the concentration of hydrogen peroxide. A linear range is found from 2.0 μM to 2.86 mM with an equation of I (μA) = $(3.3 \times 10^{-4})c$ (μM), where I is the steady-state current in μA and c is the molar concentration of hydrogen peroxide in μM. The value of K_M^{app} was calculated to 0.59 mM. The comparison of these results with that published[40−49] in Table 1 proves that such a matrix is a sensitive platform for constructing different enzyme-based biosensors for the detection of hydrogen peroxide.

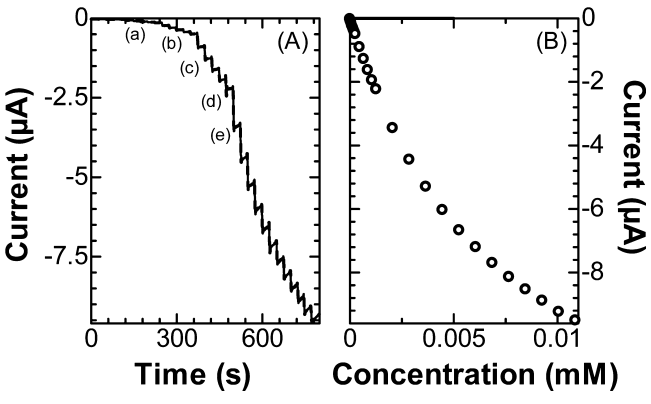

Figure 7. (A). Amperometric curve on the HRP/Au NPs/DMSA/Au electrode in 0.1 M pH 7.4 phosphate buffer after adding 2 (a), 10 (b), 40 (c), 200 (d), and 800 (e) μM hydrogen peroxide. The working potential was −0.45 V. (B) The relationship between the steady-state current and the concentration of hydrogen peroxide.

Optimization process to construct this universal matrix has been performed, including the selection of thiol and the optimization of the conditions for electrochemical deposition of gold nanoparticles. Three kinds of mercaptocarboxylic acids (MPA, MSA, and DMSA) were tried for the selection of thiol. The decision was made on the basis of the comparison of the fitted slope from the achieved amperometric curve (e.g., in Figure 4B). Under identification conditions, the slopes were about 4.6, 1.2, and 0.7 μA s^{-1} when DMSA, MSA, and MPA were applied, respectively. DMSA was thus selected. As for the deposition of gold nanoparticles on the self-assembled monolayer of DMSA-coated gold electrodes, the deposition was conducted at −0.15 V. This potential was selected from the cyclic voltammogram of $AuCl_4^-$ in the potential range of 0.2 to −0.4 V at a scan rate of 0.02 V s^{-1}, showing that the reduction of $AuCl_4^-$ starts at −0.15 V and reaches the maximum current at −0.2 V. The deposition time was decided from the fitted slope obtained as described in a previous session. When the deposition time increased from 30, 60, 90, and to 180 s, the best fitted slope was 1.4, 2.6, 4.6, and 3.2 μA s^{-1}, respectively. This is due to the enhancement of surface area of such a matrix. A decrease indicates a smaller area of the electrode, which is due to the overlap of gold nanoparticles. Therefore, a deposition potential of −0.15 V and a deposition time of 90 s was used.

The performance (stability, reproducibility, and selectivity) of such a matrix after coating with different enzymes was checked toward the monitoring of hydrogen peroxide and glucose. Their stability and the reproducibility of detecting hydrogen peroxide were examined by comparing steady-state currents of 40 μM hydrogen peroxide on the same electrode at different times and on the different electrodes but at almost the same time. Take such a matrix coated with CAT (CAT/Au NPs/DMSA/Au) as an example; the current decreased only about 6% after storing the electrode in a 0.1 M pH 7.4 phosphate buffer at 4 °C for 20 days. On different electrodes, the variation of the current is less than 4.8%. The selectivity of this matrix after being coated with different enzymes was measured as well. For example, the amperometric measurements of 20 μM glucose was conducted on the GOD/Au NPs/DMSA/Au matrix in the present of some potentially coexisting compounds in biological systems such as dopamine, ascorbic acid, acetaminophen, and uric acid. Adding these interferences (e.g., 0.4 μM dopamine, 0.5 μM uric acid, 1.6 μM ascorbic acid, and 1.6 μM acetaminophen) does not influence the detection of glucose. Therefore, such a matrix after being coated with enzymes is highly stable, reproducible, and selective for the detection of glucose and hydrogen peroxide.

CONCLUSION

In summary, a versatile matrix has been fabricated for the immobilization of enzymes and eventually for the construction of enzyme-based biosensors for the sensitive detection of glucose and hydrogen peroxide. This matrix with a three-dimensional structure was fabricated by electrochemical deposition of gold nanoparticles on the thiol monolayer self-assembled on the gold electrode. On such a matrix the electrochemistry of different enzymes (e.g., catalase, glucose oxidase, and horseradish peroxidase) and their higher catalytic ability toward the electrocatalytic reduction/oxidation of hydrogen peroxide and glucose have been realized. Amperometric monitoring of hydrogen peroxide and glucose on such a matrix has been realized with wide dynamic ranges and low detection limits. The detection can last for more than 20 days and the errors of these measurements are less than 6%. Selective monitoring of glucose is possible as well. In addition, the fabrication of such a matrix is simple and highly reproducible. These three-dimensional matrixes are therefore universal for enzyme-based biosensors. In the future, they will be scalable for immobilization of other biomolecules to develop numerous but different types of biosensors and electrochemical sensors.

AUTHOR INFORMATION

Corresponding Authors

*E-mail: qijinwan@mail.wit.edu.cn.
*E-mail: nianjun.yang@uni-siegen.de.

Present Address

[§]Department of Applied Physics, University of Fukui, Fukui 910-8507, Japan

Notes

The authors declare no competing financial interest.

ACKNOWLEDGMENTS

The authors are thankful for financial support from the National Natural Science Foundation of China (21275113, 21075096, and 21375041).

REFERENCES

(1) Hanko, M.; Bruns, N.; Rentmeister, S.; Tiller, J. C.; Heinze, J. Nanophase-Separated Amphiphilic Conetworks as Versatile Matrixes for Optical Chemical and Biochemical Sensors. *Anal. Chem.* **2006**, *78*, 6376−6383.

(2) Sota, H.; Yoshimine, H.; Whittier, R. F.; Gotoh, M.; Shinohara, Y.; Hasegawa, Y.; Okahata, Y. A Versatile Planar QCM-Based Sensor Design for Nonlabeling Biomolecule Detection. *Anal. Chem.* **2002**, *74*, 3592−3598.

(3) Huang, G. S.; Wang, M. T.; Hong, M. Y. A Versatile QCM Matrix System for Online and High-Throughput Bio-Sensing. *Analyst* **2006**, *131*, 382−387.

(4) Nuzzo, R. G.; Allara, D. L. Adsorption of Bifunctional Organic Disulfides on Gold Surfaces. *J. Am. Chem. Soc.* **1983**, *105*, 4481−4483.

(5) Porter, M. D.; Bright, T. B.; Allara, D. L.; Chidsey, C. E. D. Spontaneously Organized Molecular Assemblies. 4. Structural Characterization of n-Alkyl Thiol Monolayers on Gold by Optical Ellipsometry, Infrared Spectroscopy, and Electrochemistry. *J. Am. Chem. Soc.* **1987**, *109*, 3559−3568.

(6) Hu, K.; Bard, A. J. Use of Atomic Force Microscopy for the Study of Surface Acid-Base Properties of Carboxylic Acid-Terminated Self-Assembled Monolayers. *Langmuir* **1997**, *13*, 5114−5119.

(7) Bould, J.; Machacek, J.; Londesborough, M. G.; Macias, R.; Kennedy, J. D.; Bastl, Z.; Rupper, P.; Base, T. Decaborane Thiols as Building Blocks for Self-Assembled Monolayers on Metal Surfaces. *Inorg. Chem.* **2012**, *51*, 1685−1694.

(8) Gan, N.; Hou, J. An Amperometric Immunosensor Based on a Polyelectrolyte/Gold Magnetic Nanoparticle Supramolecular Assembly-Modified Electrode for the Determination of HIV p24 in Serum. *Molecules* **2010**, *15*, 5053−5065.

(9) Tanimura, R.; Hill, M. G.; Margoliash, E.; Niki, K.; Ohno, H.; Gray, H. B. Active Carboxylic Acid-Terminated Alkanethiol Self-Assembled Monolayers on Gold Bead Electrodes for Immobilization of Cytochromes *c*. *Electrochem Solid State Lett.* **2002**, *5*, E67−E70.

(10) Li, F.; Feng, Y.; Wang, Z.; Yang, L.; Zhuo, L.; Tang, B. Direct Electrochemistry of Horseradish Peroxidase Immobilized on the Layered Calcium Carbonate-Gold Nanoparticles Inorganic Hybrid Composite. *Biosens. Bioelectron.* **2010**, *25*, 2244−2248.

(11) Beebe, J. M.; Engelkes, V. B.; Miller, L. L.; Frisbie, C. D. Contact Resistance in Metal-Molecule-Metal Junctions Based on Aliphatic SAMs: Effects of Surface Linker and Metal Work Function. *J. Am. Chem. Soc.* **2002**, *124*, 11268−11269.

(12) Lin, Y.; Wang, J.; Wan, L. J.; Fang, X. H. Study of Fibrinogen Adsorption on Self-Assembled Monolayers on Au(111) by Atomic Force Microscopy. *Ultramicroscopy* **2005**, *105*, 129−136.

(13) Hu, L.; Zhang, Z.; Zhang, M.; Efremov, M. Y.; Olson, E. A.; de la Rama, L. P.; Kummamuru, R. K.; Allen, L. H. Self-Assembly and Ripening of Polymeric Silver-Alkanethiolate Crystals on Inert Surfaces. *Langmuir* **2009**, *25*, 9585−9595.

(14) Liu, Y.; Strauss, J.; Camesano, T. A. Adhesion Forces between Staphylococcus Epidermidis and Surfaces Bearing Self-Assembled Monolayers in the Presence of Model Proteins. *Biomaterials* **2008**, *29*, 4374−4382.

(15) Base, T.; Bastl, Z.; Havranek, V.; Machacek, J.; Langecker, J.; Malina, V. Carboranedithiols: Building Blocks for Self-Assembled Monolayers on Copper Surfaces. *Langmuir* **2012**, *28*, 2518−12526.

(16) Schmidt, C.; Witt, A.; Witte, G. Tailoring the Cu(100) Work Function by Substituted Benzenethiolate Self-Assembled Monolayers. *J. Phys. Chem. A* **2011**, *115*, 7234−7241.

(17) Liu, K.-H.; Chen, B.-R.; Chen, S.-Y.; Liu, D.-M. Self-Assembly Behavior and Doxorubicin-Loading Capacity of Acylated Carboxymethyl Chitosans. *J. Phys. Chem. B* **2009**, *113*, 11800−11807.

(18) Zuo, S.; Wu, X.; Teng, Y.; Yuan, H.; Lan, M.; Lawrance, G. A.; Wei, G. Direct Electron Transfer of Glucose Oxidase Immobilized on a Mesoporous Silica KIT-6 Matrix to Screen-Printed Electrodes. *J. Nanosci. Nanotechnol.* **2009**, *9*, 4767−4773.

(19) Zheng, Y.; Zhang, L.; Shi, J.; Liang, Y.; Wang, X.; Jiang, Z. Mussel-Inspired Surface Capping and Pore Filling to Confer Mesoporous Silica with High Loading and Enhanced Stability of Enzyme. *Microporous Mesoporous Mater.* **2012**, *152*, 122−127.

(20) Jin, L.; Yang, K.; Yao, K.; Zhang, S.; Tao, H.; Lee, S. T.; Liu, Z.; Peng, R. Functionalized Graphene Oxide in Enzyme Engineering: a Selective Modulator for Enzyme Activity and Thermostability. *ACS Nano* **2012**, *6*, 4864−4875.

(21) Kishore, D.; Talat, M.; Srivastava, O. N.; Kayastha, A. M. Immobilization of β-Galactosidase onto Functionalized Graphene Nano-Sheets Using Response Surface Methodology and Its Analytical Applications. *PLoS One* **2012**, *7*, e40708.

(22) Li, L. H.; Zhang, W. D.; Ye, J. S.; Li, L.-H.; Zhang, W.-D.; Ye, J.-S. Electrocatalytic Oxidation of Glucose at Carbon Nanotubes Supported PtRu Nanoparticles and Its Detection. *Electroanalysis* **2008**, *20*, 2212−2216.

(23) Si, P.; Kannan, P.; Guo, L.; Son, H.; Kim, D.-H. Highly Stable and Sensitive Glucose Biosensor Based on Covalently Assembled High Density Au Nanostructures. *Biosens. Bioelectron.* **2011**, *26*, 3845−3851.

(24) Xia, Y.; Huang, W.; Zheng, J.; Niu, Z.; Li, Z. Nonenzymatic Amperometric Response of Glucose on a Nanoporous Gold Film Electrode Fabricated by a Rapid and Simple Electrochemical Method. *Biosens. Bioelectron.* **2011**, *26*, 3555−3561.

(25) Wan, Q.; Song, H.; Shu, H.; Wang, Z.; Zou, J.; Yang, N. In Situ Synthesized Gold Nanoparticles for Direct Electrochemistry of Horseradish Peroxidase. *Colloids Surf., B* **2013**, *104*, 181−185.

(26) Yang, P.; Cai, H.; Liu, S.; Wan, Q.; Wang, X.; Yang, N. Electrochemical Reduction of 2,4-Dinitrophenol on Nanocomposite Electrodes Modified with Mesoporous Silica and Poly(vitamin B_1) Films. *Electrochim. Acta* **2011**, *56*, 7097−7103.
(27) Gong, K.; Dong, Y.; Xiong, S.; Chen, Y.; Mao, L. Novel Electrochemical Method for Sensitive Determination of Homocysteine with Carbon Nanotube-Based Electrodes. *Biosens. Bioelectron.* **2004**, *20*, 253−259.
(28) Manso, J.; Mena, M. L.; Yáñez-Sedeño, P.; Pingarrón, J. Electrochemical Biosensors Based on Colloidal Gold-Carbon Nanotubes Composite Electrodes. *J. Electroanal. Chem.* **2007**, *603*, 1−7.
(29) Rong, L. Q.; Yang, C.; Qian, Q. Y.; Xia, X. H. Study of the Nonenzymatic Glucose Sensor Based on Highly Dispersed Pt Nanoparticles Supported on Carbon Nanotubes. *Talanta* **2007**, *72*, 819−824.
(30) Chen, S.; Yuan, R.; Chai, Y.; Zhang, L.; Wang, N.; Li, X. Amperometric Third-Generation Hydrogen Peroxide Biosensor Based on the Immobilization of Hemoglobin on Multiwall Carbon Nanotubes and Gold Colloidal Nanoparticles. *Biosens. Bioelectron.* **2007**, *22*, 1268−1274.
(31) Feng, J. J.; Zhao, G.; Xu, J. J.; Chen, H. Y. Direct Electrochemistry and Electrocatalysis of Heme Proteins Immobilized on Gold Nanoparticles Stabilized by Chitosan. *Anal. Biochem.* **2005**, *342*, 280−286.
(32) Jia, J.; Wang, B.; Wu, A.; Cheng, G.; Li, Z.; Dong, S. A Method to Construct a Third-Generation Horseradish Peroxidase Biosensor: Self-Assembling Gold Nanoparticles to Three-Dimensional Sol-Gel Network. *Anal. Chem.* **2002**, *74*, 2217−2223.
(33) Ambrosi, A.; Castaneda, M. T.; Killard, A. J.; Smyth, M. R.; Alegret, S.; Merkoci, A. Double-Codified Gold Nanolabels for Enhanced Immunoanalysis. *Anal. Chem.* **2007**, *79*, 5232−5240.
(34) Daniel, M. C.; Astruc, D. Gold Nanoparticles: Assembly, Supramolecular Chemistry, Quantum-Size-Related Properties, and Applications toward Biology, Catalysis, and Nanotechnology. *Chem. Rev.* **2004**, *104*, 293−346.
(35) Upadhyay, A. K.; Ting, T. W.; Chen, S. M. Amperometric Biosensor for Hydrogen Peroxide Based on Coimmobilized Horseradish Peroxidase and Methylene Green in Ormosils Matrix with Multiwalled Carbon Nanotubes. *Talanta* **2009**, *79*, 38−45.
(36) Liu, Y.; Wang, Y.; Claus, R. O. Layer-by-Layer Ionic Self-Assembly of Au Colloids into Multilayer Thin-Films with Bulk Metal Conductivity. *Chem. Phys. Lett.* **1998**, *298*, 315−319.
(37) Laviron, E. Adsorption, Autoinhibition and Autocatalysis in Polarography and in Linear Potential Sweep Voltammetry. *J. Electroanal. Chem.* **1974**, *52*, 355−365.
(38) Liu, Y.; Lei, J.; Ju, H. Amperometric Sensor for Hydrogen Peroxide Based on Electric Wire Composed of Horseradish Peroxidase and Toluidine Blue-Multiwalled Carbon Nanotubes Banocomposite. *Talanta* **2008**, *74*, 965−970.
(39) Huang, K.-J.; Niu, D.-J.; Liu, X.; Wu, Z.-W.; Fan, Y.; Chang, Y.-F.; Wu, Y.-Y. Direct Electrochemistry of Catalase at Amine-Functionalized Graphene/Gold Nanoparticles Composite Film for Hydrogen Peroxide Sensor. *Electrochim. Acta* **2011**, *56*, 2947−2953.
(40) Yuan, S.; Yuan, R.; Chai, Y.; Zhuo, Y.; Yang, X.; Yuan, Y. Enzyme Biosensor Based on the Immobilization of HRP on SiO_2/BSA/Au Composite Nanoparticles. *Appl. Biochem. Biotechnol.* **2010**, *162*, 2189−2196.
(41) Chico, B.; Camacho, C.; Pérez, M.; Longo, M. A.; Sanromán, M. A.; Pingarrón, J. M.; Villalonga, R. Polyelectrostatic Immobilization of Gold Nanoparticles-Modified Peroxidase on Alginate-Coated Gold Electrode for Mediatorless Biosensor Construction. *J. Electroanal. Chem.* **2009**, *629*, 126−132.
(42) Shamsipur, M.; Asgari, M.; Mousavi, M. F.; Davarkhah, R. A Novel Hydrogen Peroxide Sensor Based on the Direct Electron Transfer of Catalase Immobilized on Nano-Sized NiO/MWCNTs Composite Film. *Electroanalysis* **2012**, *24*, 357−367.
(43) Thandavan, K.; Gandhi, S.; Sethuraman, S.; Rayappan, J. B.; Krishnan, U. M. A Novel Nanostructured Iron Oxide-Gold Bioelectrode for Hydrogen Peroxide Sensing. *Nanotechnology* **2011**, *22*, 265505.
(44) Ammam, M.; Fransaer, J. AC-Electrophoretic Deposition of Metalloenzymes: Catalase as a Case Study for the Sensitive and Selective Detection of H_2O_2. *Sens. Actuators B* **2011**, *160*, 1063−1069.
(45) Jiang, H.-J.; Yang, H.; Akins, D. L. Direct Electrochemistry and Electrocatalysis of Catalase Immobilized on a SWNT-Nanocomposite Film. *J. Electroanal. Chem.* **2008**, *623*, 181−186.
(46) Di, J.; Zhang, M.; Yao, K.; Bi, S. Direct Voltammetry of Catalase Immobilized on Silica Sol-Gel and Cysteine Modified Gold Electrode and Its Application. *Biosens. Bioelectron.* **2006**, *22*, 247−252.
(47) Wu, F.; Hu, Z.; Xu, J.; Tian, Y.; Wang, L.; Xian, Y.; Jin, L. Immobilization of Horseradish Peroxidase on Self-Assembled (3-Mercaptopropyl)-Trimethoxysilane Film: Characterization, Direct Electrochemistry, Redox Thermodynamics and Biosensing. *Electrochim. Acta* **2008**, *53*, 8238−8244.
(48) Ma, L.; Yuan, R.; Chai, Y.; Chen, S. Amperometric Hydrogen Peroxide Biosensor Based on the Immobilization of HRP on DNA-Silver Nanohybrids and PDDA-Protected Gold Nanoparticles. *J. Mol. Catal. B: Enzym.* **2009**, *56*, 215−220.
(49) Villalonga, R.; Díez, P.; Yáñez-Sedeño, P.; Pingarrón, J. M. Wiring Horseradish Peroxidase on Gold Nanoparticles-Based Nanostructured Polymeric Network for the Construction of Mediatorless Hydrogen Peroxide Biosensor. *Electrochim. Acta* **2011**, *56*, 4672−4977.
(50) Wang, J. Electrochemical Glucose Biosensors. *Chem. Rev.* **2008**, *108*, 814−825.
(51) Chen, C.; Xie, Q.; Yang, D.; Xiao, H.; Fu, Y.; Tan, Y.; Yao, S. Recent Advances in Electrochemical Glucose Biosensors: a Review. *RSC Adv.* **2013**, *2*, 4473−4491.
(52) Li, J.; Yuan, R.; Chai, Y. Simple Construction of an Enzymatic Glucose Biosensor Based on a Nanocomposite Film Prepared in One Step from Iron Oxide, Gold nanoparticles, and Chitosan. *Microchim. Acta* **2011**, *173*, 369−374.
(53) Zhong, H.; Yuan, R.; Chai, Y.; Li, W.; Zhong, X.; Zhang, Y. In Situ Chemo-Synthesized Multi-Wall Carbon Nanotube-Conductive Polyaniline Nanocomposites: Characterization and Application for a Glucose Amperometric Biosensor. *Talanta* **2011**, *85*, 104−111.
(54) Fang, B.; Zhang, C.; Wang, G.; Wang, M.; Ji, Y. A Glucose Oxidase Immobilization Platform for Glucose Biosensor Using ZnO Hollow Nanospheres. *Sens. Actuators B* **2011**, *155*, 304−310.
(55) Si, P.; Kannan, P.; Guo, L.; Son, H.; Kim, D.-H. Highly Stable and Sensitive Glucose Biosensor Based on Covalently Assembled High Density Au Nanostructures. *Biosens. Bioelectron.* **2011**, *26*, 3845−3851.
(56) Zeng, Q.; Cheng, J. S.; Liu, X. F.; Bai, H. T.; Jiang, J. H. Palladium Nanoparticle/Chitosan-Grafted Graphene Nanocomposites for Construction of a Glucose Biosensor. *Biosens. Bioelectron.* **2011**, *26*, 3456−3463.
(57) Tang, H.; Yan, F.; Tai, Q.; Chan, H. L. The Improvement of Glucose Bioelectrocatalytic Properties of Platinum Electrodes Modified with Electrospun TiO_2 Nanofibers. *Biosens. Bioelectron.* **2010**, *25*, 1646−1651.
(58) Nejadnik, M. R.; Deepak, F. L.; Garcia, C. D. Adsorption of Glucose Oxidase to 3-D Scaffolds of Carbon Nanotubes: Analytical Applications. *Electroanalysis* **2011**, *23*, 1462−1469.
(59) Fu, G.; Yue, X.; Dai, Z. Glucose Biosensor Based on Covalent Immobilization of Enzyme in Sol-Gel Composite Film Combined with Prussian Blue/Carbon Nanotubes Hybrid. *Biosens. Bioelectron.* **2011**, *26*, 3973−3976.
(60) Salimi, A.; Sharifi, E.; Noorbakhsh, A.; Soltanian, S. Immobilization of Glucose Oxidase on Electrodeposited Nickel Oxide Nanoparticles: Direct Electron Transfer and Electrocatalytic Activity. *Biosens. Bioelectron.* **2007**, *22*, 3146−3153.
(61) Wang, Z.; Liu, S.; Wu, P.; Cai, C. Detection of Glucose Based on Direct Electron Transfer Reaction of Glucose Oxidase Immobilized on Highly Ordered Polyaniline Nanotubes. *Anal. Chem.* **2009**, *81*, 1638−1645.
(62) Zuo, S.; Wu, X.; Teng, Y.; Yuan, H.; Lan, M.; Lawrance, G. A.; Wei, G. Direct Electron Transfer of Glucose Oxidase Immobilized on a

Mesoporous Silica KIT-6 Matrix to Screen-Printed Electrodes. *J. Nanosci. Nanotechnol.* **2009**, *9*, 4767−4673.
(63) You, C.; Yan, X.; Kong, J.; Zhao, D.; Liu, B. Bicontinuous Gyroidal Mesoporous Carbon Matrix for Facilitating Protein Electrochemical and Bioelectrocatalytic Performances. *Talanta* **2011**, *83*, 1507−1515.
(64) Wu, S.; Liu, G.; Li, P.; Liu, H.; Xu, H. A High-Sensitive and Fast-Fabricated Glucose Biosensor Based on Prussian Blue/Topological Insulator Bi_2Se_3 Hybrid Film. *Biosens. Bioelectron.* **2012**, *38*, 289−294.
(65) Yin, H.; Zhou, Y.; Meng, X.; Shang, K.; Ai, S. One-Step "Green" Preparation of Graphene Nanosheets and Carbon Nanospheres Mixture by Electrolyzing Graphite Rob and Its Application for Glucose Biosensing. *Biosens. Bioelectron.* **2011**, *30*, 112−117.
(66) Li, W.; Yuan, R.; Chai, Y.; Zhong, H.; Wang, Y. Study of the Biosensor Based on Platinum Nanoparticles Supported on Carbon Nanotubes and Sugar-Lectin Biospecific Interactions for the Determination of Glucose. *Electrochim. Acta* **2011**, *56*, 4203−4208.
(67) Yang, L.; Xiong, H.; Zhang, X.; Wang, S.; Zhang, X. Direct Electrochemistry of Glucose Oxidase and Biosensing for Glucose Based on Boron-Doped Carbon-Coated Nickel Modified Electrode. *Biosens. Bioelectron.* **2011**, *26*, 3801−3805.
(68) Zhai, Y.; Zhai, S.; Chen, G.; Zhang, K.; Yue, Q.; Wan, L.; Liu, J.; Jia, J. Effects of Morphology of Nanostructured ZnO on Direct Electrochemistry and Biosensing Properties of Glucose Oxidase. *J. Electroanal. Chem.* **2011**, *656*, 198−205.
(69) Yang, J. Electrochemical Synthesis of Reduced Graphene Sheet-AuPd Alloy Nanoparticle Composites for Enzymatic Biosensing. *Biosens. Bioelectron.* **2011**, *29*, 159−166.
(70) Salimi, A.; Noorbakhsh, A. Layer by Layer Assembly of Glucose Oxidase and Thiourea onto Glassy Carbon Electrode: Fabrication of Glucose Biosensor. *Electrochim. Acta* **2011**, *56*, 6097−6105.
(71) Liu, D.; Zhang, X.; You, T. Electrochemical Performance of Electrospun Free-Standing Nitrogen-Doped Carbon Nanofibers and Their Application for Glucose Biosensing. *ACS Appl. Mater. Interfaces* **2014**, *6*, 6275−6280.
(72) Wang, J.-Y.; Chen, L.-C.; Ho, K.-C. Synthesis of Redox Polymer Nanobeads and Nanocomposites for Glucose Biosensors. *ACS Appl. Mater. Interfaces* **2013**, *5*, 7852−7861.
(73) Wu, J.; Yin, L. Platinum Nanoparticle Modified Polyaniline-Functionalized Boron Nitride Nanotubes for Amperometric Glucose Enzyme Biosensor. *ACS Appl. Mater. Interfaces* **2011**, *3*, 4354−4362.
(74) Guo, C. X.; Sheng, Z. M.; Shen, Y. Q.; Dong, Z. L.; Li, C. M. Thin-Walled Graphitic Nanocages As a Unique Platform for Amperometric Glucose Biosensor. *ACS Appl. Mater. Interfaces* **2010**, *2*, 2481−2484.
(75) Hu, C.; Yang, D.-P.; Zhu, F.; Jiang, F.; Shen, S.; Zhang, J. Enzyme-Labeled Pt@BSA Nanocomposite as a Facile Electrochemical Biosensing Interface for Sensitive Glucose Determination. *ACS Appl. Mater. Interfaces* **2014**, *6*, 4170−4178.
(76) Ko, Y.-S.; Kwon, Y.-U. Mesoporous Zirconia Thin Films with Three-Dimensional Pore Structures and Their Application to Electrochemical Glucose Detection. *ACS Appl. Mater. Interfaces* **2013**, *5*, 3599−3606.
(77) Lee, S.; Ringstrand, B. S.; Stone, D. A.; Firestone, M. A. Electrochemical Activity of Glucose Oxidase on a Poly(ionic liquid)−Au Nanoparticle Composite. *ACS Appl. Mater. Interfaces* **2012**, *4*, 2311−2317.
(78) Jia, X.; Hu, G.; Nitze, F.; Barzegar, H. R.; Sharifi, T.; Tai, C.-W.; Wågberg, T. Synthesis of Palladium/Helical Carbon Nanofiber Hybrid Nanostructures and Their Application for Hydrogen Peroxide and Glucose Detection. *ACS Appl. Mater. Interfaces* **2013**, *5*, 12017−12022.
(79) Yang, H.-W.; Hua, M.-Y.; Chen, S.-L.; Tsai, R.-Y. Reusable Sensor Based on High Magnetization Carboxyl-Modified Graphene Oxide with Intrinsic Hydrogen Peroxide Catalytic Activity for Hydrogen Peroxide and Glucose Detection. *Biosens. Bioelectron.* **2013**, *41*, 172−179.